Structure and properties of layer-by-layer self-assembled chitosan/lignosulfonate multilayer film

Hui Luo, Qing Shen *, Fan Ye, Yi-Fei Cheng, Mebrahtu Mezgebe, Rui-Juan Qin

State Key Laboratory for Modification of Chemical Fiber and Polymers, Polymer Department of Donghua University, 2999 Renmin Rd. N. Songjiang, 201620, Shanghai, PR China

ARTICLE INFO

ABSTRACT

The formation of polycation chitosan, CS, with polyanion lignosulfonate, LGS, multilayer films based on layer-by-layer self-assembly method was investigated by several techniques. UV absorption spectra showed that the growth of both CS and LGS layers followed the exponential model. The film surface wettability was found alternated depending on the surface properties of these two materials because the contact angle is smaller for the CS layer and greater for the LGS layer while the surface free energy is known greater for the former and smaller for the latter. AFM images indicated that the surface roughness of these layers was in nanosize and was increased with the layer number due to the aggregation. The field emission scanning electron microscope photograph showed that the average thickness of each layer was about 5–6 nm.

© 2012 Elsevier B.V. All rights reserved.

1. Introduction

Layer-by-layer self-assembly of oppositely charged polyelectrolytes as multilayer films has been broadly studied and reported elsewhere [1–8]. In such case, the known driving forces are the electrostatic interaction, dipole interactions, H-bonds, dispersion and van der Waals interactions [1–10]. The main factors, e.g. the ionic strength, pH [11,12], chain conformation [13], charge density [14], concentration [15] and the secondary interactions [16] have been recognized influence the film building process.

According to literature, the layer-by-layer self-assembled multilayers follow the linear growth model [5,6] or the exponent model [10–16]. However, the presented models are found to vary the forms because the parameters are varied according to used methods [1–19].

Chitosan, CS, [11,20,21] and lignosulfonates, LGS, [22–24] are two natural polyelectrolytes with positive and negative charges, respectively. The cationic CS and anionic LGS both have been broadly applied [11,17–30], and uniquely assembled with other materials, e.g. CS with anionic hyaluronan (HA) [11], dextran sulfate [25], poly(thiophene-3-acetic acid) (PTAA) [26], polyoxometalate [27] and heparin [28], and the LGS with poly(o-ethoxyaniline) [29] and laccase [30]. Considering the CS and LGS have never been together self-assembled to form a multilayer film, and such film is expected to have good bio-properties as the CS/HA [11], it is therefore proposed to layer-by-

layer self-assemble the CS/LGS multilayer films and to study its structure and properties. Experimentally, we applied the UV spectroscopy to study the layer growth process, and FTIR, contact angle measurement, AFM and FESEM, respectively, to characterize the structure and properties of self-assembled CS/LGS multilayer films' Islets.

2. Experimental

2.1. Materials

A commercial powder CS in microsize obtained from Weifang Kehai Chitosan Co., Ltd, China was used as received. The molecular weight and deacetylation degree of this CS sample were known from the producer to be about 3×10^5 g/mol and 95%, respectively.

The Ca–LGS which is also a commercial powder in microsize obtained from Jiangmen Sugar Cane Chemical Factory, Guangdong of China was used as received. According to the producer, this LGS has the lignin component $\geq 55\%$, deoxidized sugars $\leq 12\%$, water insoluble components $\leq 1.5\%$, moisture $\leq 9\%$ and pH of about 5 [24].

A concentrated HAc, commercial H_2SO_4 and 30% H_2O_2 as well as other chemicals in analytical grade were purchased from a local chemical store at Shanghai and used as received.

A lab-made distilled water was always used in this case.

2.2. Preparation of CS, LGS solutions and substrate

The CS/acetic acid solution and LGS/water solution were initially prepared, respectively, and both in the same concentrations, e.g. 2 mg/mL, and pH, e.g. 4.1.
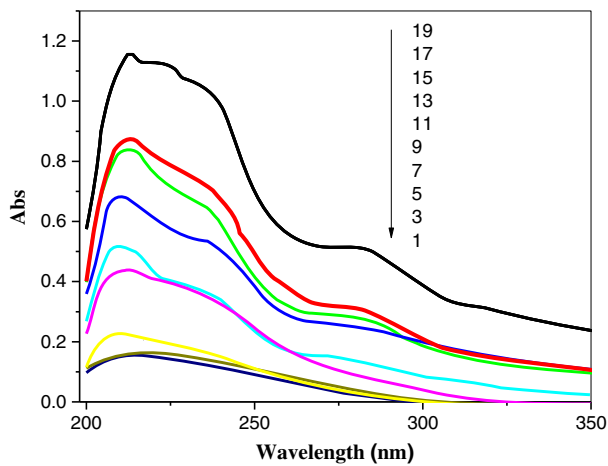
Fig. 1. UV absorption spectra of layer-by-layer self-assembled $(CS/LGS)_n$ multilayer films.

The lab-scale hydrophilic glass slides were initially pretreated by sonicating them in 98% H_2SO_4/30% H_2O_2 (7:3) solution (piranha solution) for 1 h, then immersed in a H_2O/H_2O_2/NH_4OH (5:1:1) solution for another 1 h. Before application, all these substrates were dried by hot air.

2.3. Layer-by-layer self-assembly of $(CS/LGS)_n$ multilayer films

The layer-by-layer self-assembled CS/LGS multilayer films were fabricated in the same way as the literature introduced [2]. Initially, the glass substrate was immersed in the CS solution (2 mg/mL, pH 4.1) for 10 min to build up the first layer then air dried to form a CS-coated substrate. After that, the CS-coated substrate was moved to the LGS solution (2 mg/mL, pH 4.1) for dipping 10 min to build up the second layer and then also air dried to form the LGS layer. Then, the other CS and LGS layers were continuously built up, respectively, in the same way as above. In this case, the multilayer film was defined as $(CS/LGS)_n$, where the n represents the layer number.

All these steps were performed under air stream flow condition.

2.4. Characterization

The self-assembly process was in situ determined by UV spectroscopy (Hitachi U-4000 spectrophotometer) equipped with an integrating
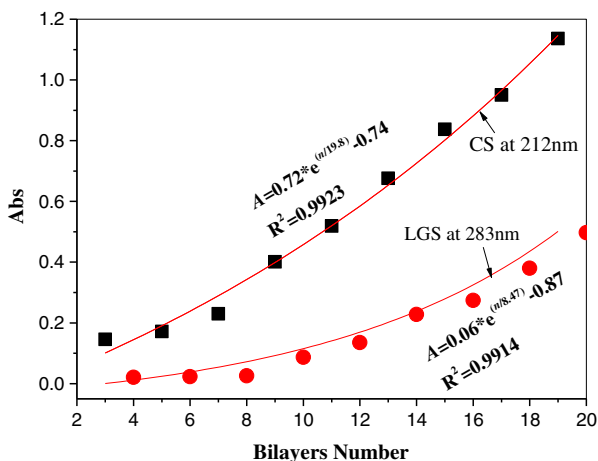
Table 1
A summary of the layer growth constants for assembling CS and LGS layers determined on the basis of Eq. (1).

Samples	a	b	c
CS	0.72	19.8	0.74
LGS	0.06	8.47	0.87

sphere detection system due to the UV absorption intensity proportional to the layer number as seen in literature [31–33].

The FTIR spectra of multilayer films were recorded using a NEXUS-670 (Nicolet Co., Ltd) spectrometer in transmission mode by aligning the film on a silicon wafer substrate (1–2 cm^2) at a Brewster's angle of 75° with respect to the incident beam.

The wetting of films was characterized by means of the sessile drop contact angle measurement using the OCA40 Micro (Dataphysics Co., Ltd). During the measurement, the droplet volume was controlled constantly at about 1 μL for each drop and the temperature was controlled in constant, 25 °C.

The surface topography and roughness of the multilayer film was analyzed using a NanoScope IV (Veeco Co., Ltd) AFM with a tapping mode.

The cross-section of the multilayer film was analyzed by field emission scanning electron microscope, FESEM, (S-4800, HITACHI Co., Ltd.,) at an accelerating voltage of 5.0 kV.

3. Results and discussion

3.1. Layer growth and related model

Taking UV adsorption intensity as a function of the layer number, Fig. 1 showed several curves corresponding to the assembled layers where the odd layer is related to the CS and the even layer is related to the LGS, respectively. Since the intense peak centered at about 212 nm due to the electrons' transition from the amide of CS and at about 282 nm due to the benzene ring of LGS, respectively, the intensities of these two peaks are therefore taken as a function of related layer number similarly as the literature introduced [7,11,13] to present a new plot in Fig. 2. According to Fig. 2, we obtained the layer growth model on both CS and LGS (Eq. (1)), which indicated both the assembled CS and LGS layers following the exponent models [10–16].
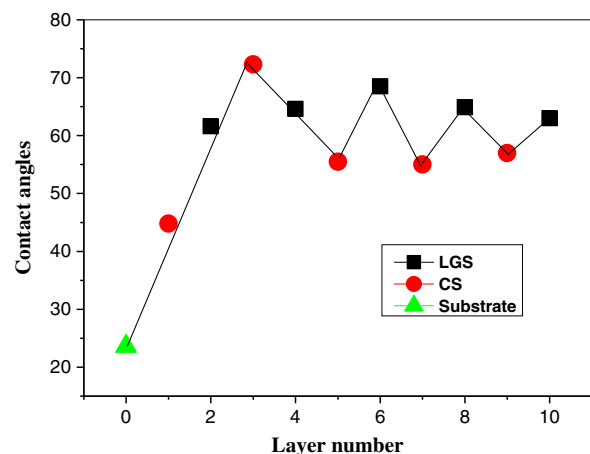
$$Y = a \times \exp(N/b) - c \qquad (1)$$

Fig. 2. A plot of the UV absorption intensity of CS and LGS related peaks vs. their layer numbers, respectively.

Fig. 3. Wettability of CS/LGS multilayer films, where the even layer corresponds to LGS as the outermost layer and the odd layer correspond to CS as the outermost layer.
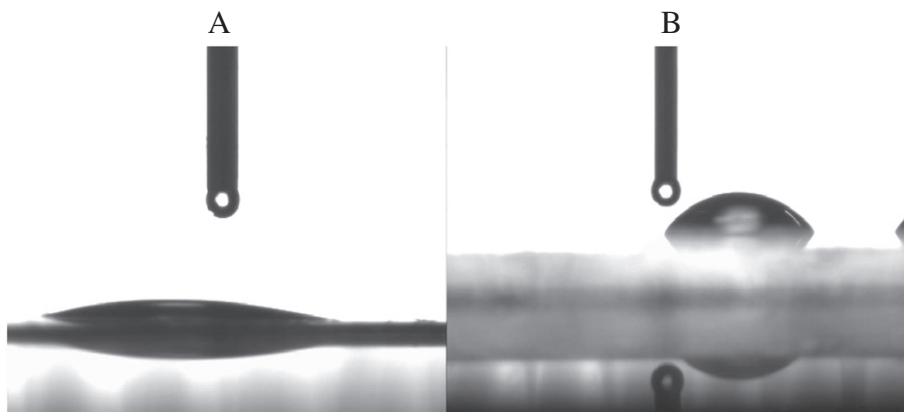
Fig. 4. Photographs of water drop on the surfaces of glass (A), and eight layer (B), respectively.

where Y is the absorption value which could be varied according to different measurements such as the film mass, thickness and other structure or property related parameters; N is the layer number. The presented three Latin letters, a, b and c are constants, respectively.

To compare Eq. (1) with literature reported equations suggested that Y can represent various physical parameters, e.g. the weight, thickness, adsorption and others [10–16]. Table 1 presented the constants determined from this work which are considerably relating to some meanings of this assembly system [10–16].

3.2. Structure and properties of CS/LGS multilayer films

3.2.1. Wettability

The surface wettability is usually very sensitive to the compositions of the outermost layer, and it is availably known by contact angle measurement [25,27,34]. In Fig. 3, the contact angles between water and the surfaces of the substrate (zero layer), CS and LGS, were presented, respectively. Since the contact angle on the glass surface is very small, this suggests the glass surface is hydrophilic. The contact angles on the initial four layers are found to follow a linear fit ignoring the material properties. This wetting behavior is probably due to these layers assembled without uniformity due to the slow interdiffusion. This initial wetting behavior is also possible due to

Fig. 5. FTIR spectra of native CS, LGS and (CS/LGS)$_{22}$ multilayer films.

the original roughness of the glass surface. Since the assembly of the five layers, it was found that the contact angles on the surface of both CS and LGS have a greater increase as compared with that on the glass surface and the contact angle is always greater for the LGS layer and smaller for the CS layer to present a zigzag aspect. This wetting behavior is interesting because this suggests that the CS layer is hydrophilic and the LGS layer is hydrophobic. However, this is possible and supported by our previous investigation of the surface properties of both CS and LGS, because we found the surface free energy is smaller for LGS [24] and greater for CS [35]. Therefore, it can be concluded that the zig-zag wetting behavior is mainly dominated by the surface properties of these used materials.

In order to see the detailed wetting process on water drop contact with the surface of glass and self-assembled layer surface, Fig. 4 presented two photographs where the contact angle is smaller on the glass surface and greater on the layer surface obviously.

3.2.2. FTIR spectra

The FTIR spectra of self-assembled CS/LGS multilayer films were presented in Fig. 5 where the native CS and LGS samples are compared. CS exhibits strong peaks at 3410 cm^{-1} due to the O–H or N–H vibration [20–22], at 2930 cm^{-1} due to the C–H stretching, at 1640 cm^{-1} due to the carbonyl asymmetric stretching vibration [20–22], at 1510 cm^{-1} corresponding to the amide II and at 1040 cm^{-1} due to the C–O vibration [22]. LGS presented intense peaks at 1050 cm^{-1} due to the S=O stretching [24], at 1420 cm^{-1} due to an antisymmetric stretching of the methyl and methylene, and at 1580 cm^{-1} due to the C=C stretching of phenyl [24,29]. Since (CS/LGS)$_{22}$ multilayer film showed an infrared band at 897 cm^{-1} assigned to the ring stretching while this peak was not observed for both CS and LGS (Fig. 5), this suggests that the interpenetration was occurred during the self-assembly of CS/LGS multilayer film. In other words, this means the CS/LGS multilayer film was self-assembled mainly by opposite charges-induced **interpenetration. This finding is significant for self-assembling opposite changes-based natural polyelectrolytes.

Because the (CS/LGS)$_{22}$ film also exhibits some characteristic IR peaks at 1080, 1421 and 1640 cm^{-1} due to them broad as comparing with the native CS and LGS (Fig. 5). In fact, in Fig. 5 the H-bonding-based peak appeared at 3410 cm^{-1} was found narrow for both CS and LGS while broad for CS/LGS film (Fig. 5, right) is a suggestion of this multilayer film was also made by H-bonding.

3.2.3. AFM image

The AFM image of prepared film was initially focused on the fourth (Fig. 6 A,B) and eighth layers (Fig. 6 C,D) both taking the LGS as the outermost. Though these surfaces presented similar bright spots, the difference is clearly because the eight layer is roughly
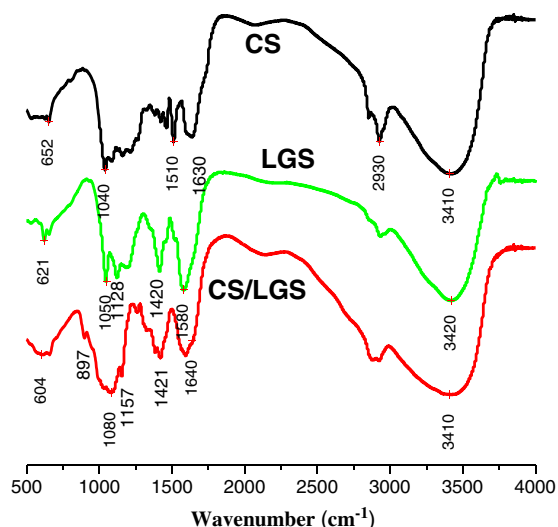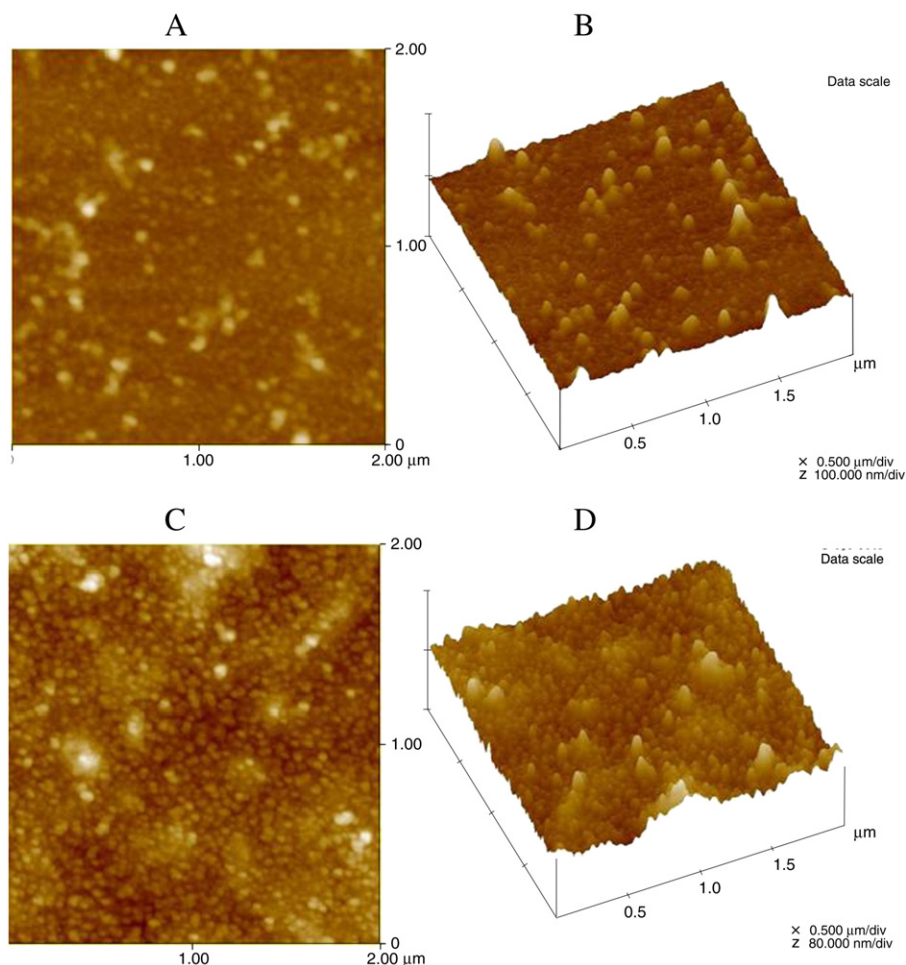
A

B

C

D

Fig. 6. AFM images of the morphology of $(CS/LGS)_4$ and $(CS/LGS)_8$ multilayer films both taking the LGS as the outermost. Images in $2 \times 2 \, \mu m^2$ with the z scales were shown.

than the fourth layer. This difference is also an interest because this implies that these two opposite charges-based natural polyelectrolytes aggregated during the self-assembly process. Though this is in good agreement with literature [36], the further induced consideration is that the fact is that the spot size is increased with the layer number to suggest the aggregation gradually increased with the self-assembly process. This assumption was subsequently proven by determined surface roughness, R_q, of the layers at fourth, eighth (Fig. 6) and eighteen (Fig. 7), respectively, all contributed by LGS. According to associated software, these layers related R_q was at 4.56, 6.13 and 7.70 nm, respectively. Therefore, it is known that the self-assembly of opposite charges-based natural polyelectrolytes would cause the aggregation and this leads the surface roughness increased with the layer number increase. However, this surface roughness seems to be without influence the surface wettability because Fig. 3 showed constant contact angles on both the CS and LGS layers. In other words, this indicated that the influence from the nanoscale roughness is quite small on sessile drop contact angle measurement.

The AFM image was furthermore focused on the comparison of the layer surface contributed by both CS and LGS as the outermost. Fig. 7 showed that the aggregator size is smaller on the LGS layer surface (Fig. 7 top) and greater on the CS layer surface (Fig. 7 bottom). Additionally, the comparison of the CS and LGS layer surfaces (Fig. 7) we found that the bright spots are contributed by CS because of the polyanions-based LGSs mostly adsorbed [32]. This phenomenon is interested because it furthermore implied that the LGS particles are easily aggregated due to the electrostatic and H-bonding

forces. In other words, this indicates that the polyelectrolytes bearing opposite charges are directly mixed in water to form the aggregates [32].

3.2.4. FESEM

The FESEM photographs of the cross-section of $(CS/LGS)_{36}$ film was showed in Fig. 8. We found that the each layer thickness was not clearly as the same as literature reported [36]. The reason is that the single layer is very thin, its clear layer thickness is not easy to observe by SEM [37]. In terms of the total thickness of the cross-section e.g. approximately 200 nm, the averaged single layer thickness was estimated to be at 5–6 nm, which is similarly as the surface roughness value. According to Fig. 8, the interface between the glass substrate and film has some holes, this suggests that the CS/LGS film was initially self-assembled mainly by the electrostatic force, then by the H-bonding force. Since the film thickness of CS/HA is about 2.4 μm for 36 layers [11], a comparison of the CS/LGS film indicated that our prepared sample with smaller later thickness. This is an interest because this suggests that the CS/LGS multilayer film may apply to some cases where the nanoscale required.

To understand a multilayer film formed by two opposite charges, Paterno et al. [29] have indicated the formed is a strong complex because they found the surface potential for the positive poly(o-ethoxyaniline), POEA, at + 170 mV, for the negative LGS at − 60 mV, while for the assembled layer film of POEA/LGS at + 290 mV which is higher than the original POEA.
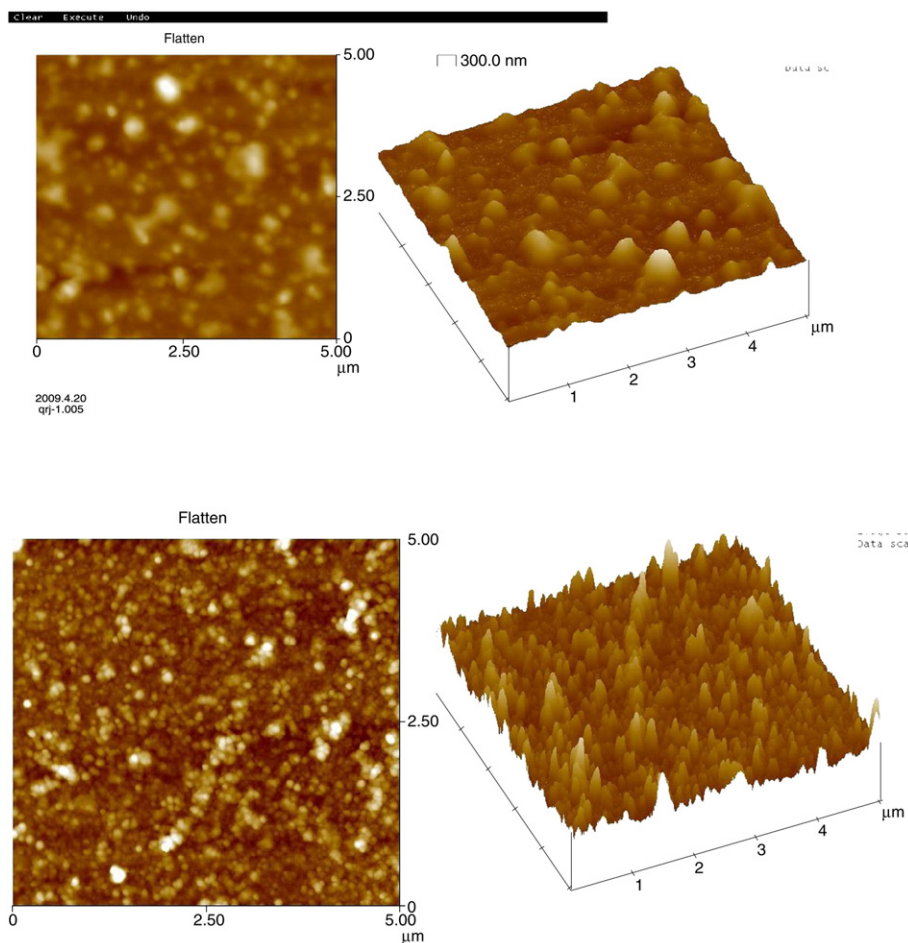
Fig. 7. Comparison of the AFM images of CS/LGS multilayer films at 17 and 18 layers corresponding to the outermost with CS and LGS, respectively. Images in 2×2 μm² with the z scales were shown.
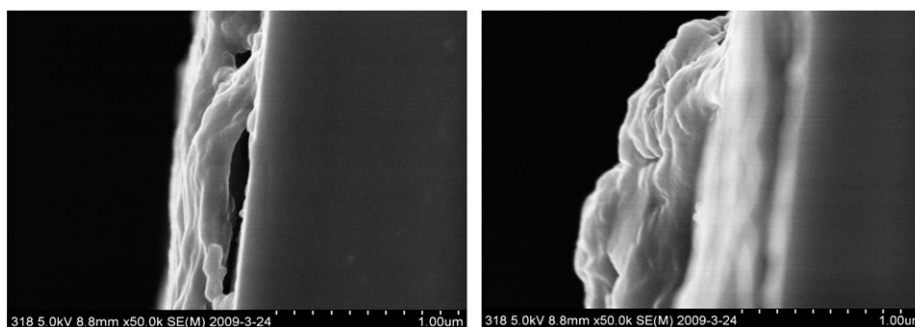

Fig. 8. FESEM image of the cross-section of $(CS/LGS)_{36}$ multilayer films.

4. Conclusion

Experiment proven that the opposite charges-based CS and LGS are capably layer-by-layer self-assembled to form the multilayer films, and when the main driving forces are the electrostatic attraction and hydrogen bonding. The self-assembly of both the CS and LGS layers follow the same universal model: $Y = ae^{N/b}-c$, where Y is the absorption value or others as mentioned above, N is the layer number, and the three Arabic letters, a, b and c are constants. The wetting behavior of CS/LGS multilayer films at the initial four layers follow linear fit to increase the contact angles with the layer number and since the five layer the contact angles presented the zigzag aspect where the greater contact angle is always greater for LGS layer and smaller for CS layer. AFM images proven that the film surface roughness is gradually increased with the layer number due to the aggregation, and the roughness value is similar as the layer thickness, e.g. about 5–6 nm.

References

[1] V. Ball, F. Bernsmann, C. Betscha, C. Maechling, S. Kauffmann, B. Senger, J.C. Voegel, P. Schaaf, N. Benkirane-Jessel, Langmuir 25 (2009) 3593.
[2] E. Hubsch, V. Ball, B. Senger, G. Decher, J.C. Voegel, P. Schaaf, Langmuir 20 (2004) 1980.
[3] J. Cho, J.F. Quinn, F. Caruso, J. Am. Chem. Soc. 126 (2004) 2270.
[4] M. Salomaki, J. Kankare, Biomacromolecules 10 (2009) 294.
[5] M. Ferreirat, M.F. Rubner, Macromolecules 28 (1995) 7107–7114.
[6] A. van Frank, K. Lutz, T. Bernd, Thin Solid Films 3 (1998) 762–766.

[7] S.A. Sukhishvili, Curr. Opin. Colloid Interface Sci. 10 (2005) 37–44.

[8] A. Jad, B. Joseph, Curr. Opin. Colloid Interface Sci. 11 (2006) 324–329.

[9] W. Barry, Y. Ninham, Langmuir 13 (1997) 2097–2108.

[10] N. Laugel, C. Betscha, M. Winterhalter, J.C. Voegel, P. Schaaf, V. Ball, J. Phys. Chem. B 110 (2006) 19443–19449.

[11] L. Richert, P. Lavalle, E. Payan, X.Z. Shu, G.D. Prestwich, J.F. Stoltz, P. Scha, J.C. Voegel, C. Picart, Langmuir 20 (2004) 448–458.

[12] T. Stephan, B. Joseph, Macromolecules 34 (2001) 3736–3740.

[13] B. Soheil, E.K. Christopher, J.K. Matt, Biomacromolecules 9 (2008) 2021–2028.

[14] A. Svetlana, K. Eugenia, I. Vladimir, Macromolecules 39 (2006) 8873–8881.

[15] G.M. Liu, S.R. Zou, F. Li, G.Z. Zhang, J. Phys. Chem. B 112 (2008) 4167–4171.

[16] K. Kamelia, M. Viktoria, P. Ivana, R. Tsetska, Biomacromolecules 9 (2008) 1242–1247.

[17] H. Kim, M.W. Urban, Langmuir 14 (1998) 7235–7244.

[18] A. Voigt, H. Lichtenfeld, G.B. Sukhorukov, H. Zastrow, E. Donath, H. BaumLer, H. Mohwald, Ind. Eng. Chem. Res. 38 (1999) 4037–4043.

[19] P. Rilling, T. Walter, R. Pommersheim, W. Vogt, J. Membr. Sci. 129 (1997) 283–287.

[20] Q. Yang, F.D. Dou, B.R. Liang, Q. Shen, Carbohydr. Polym. 59 (2005) 205–210.

[21] Q. Yang, F.D. Dou, B.R. Liang, Q. Shen, Carbohydr. Polym. 61 (2005) 393–398.

[22] M.W. Anthonsen, O. Smidsrød, Carbohydr. Polym. 26 (1995) 303–305.

[23] S.A. Gundersen, M.H. Ese, J. Sjoblom, Colloids Surf. A 182 (2001) 199–218.

[24] Q. Shen, T. Zhang, M.F. Zhu, Colloids Surf. A 320 (2008) 57.

[25] T. Serizawa, M. Yamaguchi, M. Akashi, Biomacromolecules 3 (2002) 724–731.

[26] C.A. Constantine, S.V. Mello, A. Dupont, X. Cao, D. Santos Jr., O.N. Oliveira Jr., F.T. Strixino, E.C. Pereira, T.C. Cheng, J.J. Defrank, R.M. Leblanc, J. Am. Chem. Soc. 125 (2003) 1805–1809.

[27] Y.H. Feng, Z.G. Huang, J. Peng, J. Li, B. Xie, L. Li, H.Y. Ma, E.B. Wuang, Mater. Lett. 60 (2006) 1588–1593.

[28] Q. Ruan, Y. Zhu, F. Li, J. Xiao, Y. Zeng, F. Xu, J. Colloid Interface Sci. 333 (2009) 725–733.

[29] L.G. Paterno, C.J.L. Constantino, O.N. Oliveira Jr., L.H.C. Mattoso, Colloids Surf. B 23 (2002) 257–262.

[30] C. Crestini, R. Perazzini, R. Saladino, Appl. Catal. A 372 (2010) 115–123.

[31] S.P. Jiang, Z.C. Liu, Z.Q. Tian, Adv. Mater. 18 (2006) 1068–1072.

[32] P. Schuetz, F. Caruso, Colloids Surf., A 207 (2002) 33–40.

[33] L.C. Guerentea, J. Desbrieres, J. Fatisson, P. Labbe, M.C. Rodriguez, G. Rivas, Electrochim. Acta 50 (2005) 2865–2877.

[34] L. Wågberg, G. Decher, M. Norgren, Langmuir 24 (2008) 784–795.

[35] W. Shao, X. Wang, H.G. Ding, Q. Shen, Chin. J. Cellul. Sci. Technol. 14 (1) (2006) 35–40.

[36] M.J. McShane, Y.M. Lvov, Dekker Encyclopedia of Nanoscience and Nanotechnology, Marcel, 2004, pp. 1–16.

[37] P.T. Hammond, Curr. Opin. Colloid Interface Sci. 4 (2000) 430–442.